Journal of Pharmaceutical Sciences 114 (2025) 486–496

Contents lists available at ScienceDirect

Journal of Pharmaceutical Sciences

journal homepage: www.jpharmsci.org

Pharmaceutics, Drug Delivery and Pharmaceutical Technology

Dissolution mechanisms of amorphous solid dispersions: Role of polymer molecular weight and identification of a new failure mode

Alexandru Deac[a], Chailu Que[a], Michelle L. Cousineau[a], Anura S. Indulkar[b], Yi Gao[c,*], Geoff G.Z. Zhang[a,b,d], Lynne S. Taylor[a,*]

[a] Department of Industrial and Molecular Pharmaceutics, College of Pharmacy, Purdue University, West Lafayette, IN 47907, United States
[b] Development Sciences, Research and Development, AbbVie Inc., North Chicago, IL 60064, United States
[c] Formulation Development, Drug Product Science & Technology, AbbVie Inc., North Chicago, IL 60064, United States
[d] ProPhysPharm LLC, Lincolnshire, IL 60069, United States

ARTICLE INFO

Article history:
Received 29 August 2024
Revised 14 October 2024
Accepted 14 October 2024
Available online 24 October 2024

Keywords:
Limit of congruency
Phase inversion
Nanodroplet agglomeration
Failure mode
Drug release
Polymer molecular weight
Confocal microscopy
In situ imaging

ABSTRACT

The mechanisms of drug release from amorphous solid dispersions (ASDs) are complex and not fully explored, making it difficult to optimize for in vivo performance. A recurring behavior has been the limit of congruency (LoC), a drug loading above which the ASD surface forms an amorphous drug-rich barrier in the presence of water, which hinders release, especially in non-sink conditions. Drug-polymer interactions and drug glass transition temperature were reported to affect the LoC. However, the effect of polymer molecular weight has not been explored. ASDs of clotrimazole and different molecular weight grades of poly (vinylpyrrolidone) (PVP) were studied for their release to obtain their LoC drug loadings. Failure modes underpinning the LoC were investigated using fluorescence confocal microscopy to analyze the ASD/solution interface and phase behavior of ASD films at high relative humidity. ASDs with good release formed stable drug-rich nanodroplets at the ASD/solution interface, while ASDs with poor release were limited by one of two failure modes, depending on PVP molecular weight. In Failure Mode I the nanodroplets quickly agglomerated, while in Failure Mode II the system underwent phase inversion. This work highlights the importance of identifying the mechanisms underlying the LoC to improve the release of higher drug loading ASDs.

© 2024 American Pharmacists Association. Published by Elsevier Inc. All rights are reserved, including those for text and data mining, AI training, and similar technologies.

Introduction

Amorphous solid dispersions (ASDs) are molecular mixtures of drug and polymer, which are used to increase release rate and enhance the bioavailability of poorly soluble drugs. One of the earliest commercial applications of this technique was for the product Cesamet, which was approved in the United States in 1985.[1] Despite this early approval, ASDs didn't become a widespread commercial formulation strategy until the past decade,[2] which is a direct result of the increase in the number of BCS class II and IV drugs in development.[3] The reluctance to use ASDs arises in part from their inherent metastability. The prevailing concept is that ASDs improve bioavailability through the higher solubility and dissolution rate of the thermodynamically unstable amorphous form of the drug.[4] Therefore, it is imperative to delay or prohibit drug crystallization in the solid and solution states. However, recent evidence suggests there are additional release mechanisms, unique to ASDs, which may improve bioavailability beyond the higher solubility properties of neat amorphous drug. The potential implication is a substantial in vivo performance difference among physically stable ASDs. Thus, it is important to fully understand the relationship between ASD formulation and release properties.

The bioavailability improvement observed for certain ASDs[5-7] comes from two release behaviors that have been primarily observed at low drug loading, where polymer is thought to control the release of drug. One characteristic of polymer-controlled release is that drug and polymer release congruently (i.e. together), in the same proportion as in the ASD.[8] Studies show that ASDs can have release rates that are several orders of magnitude higher than that of neat amorphous drug.[8-10] Moreover, the surface area-normalized release rate of components from these ASDs was comparable to that of the neat polymer used in the ASD. The second behavior is fast and complete release in non-sink conditions.[8] As the apparent drug concentration in solution exceeds the maximum drug supersaturation (i.e. the amorphous solubility) the solution forms drug-rich nanoparticles through a process called liquid-liquid phase separation (LLPS).[11]

* Corresponding authors.
E-mail addresses: gao.yi@abbvie.com (Y. Gao), lstaylor@purdue.edu (L.S. Taylor).

https://doi.org/10.1016/j.xphs.2024.10.026
0022-3549/© 2024 American Pharmacists Association. Published by Elsevier Inc. All rights are reserved, including those for text and data mining, AI training, and similar technologies.

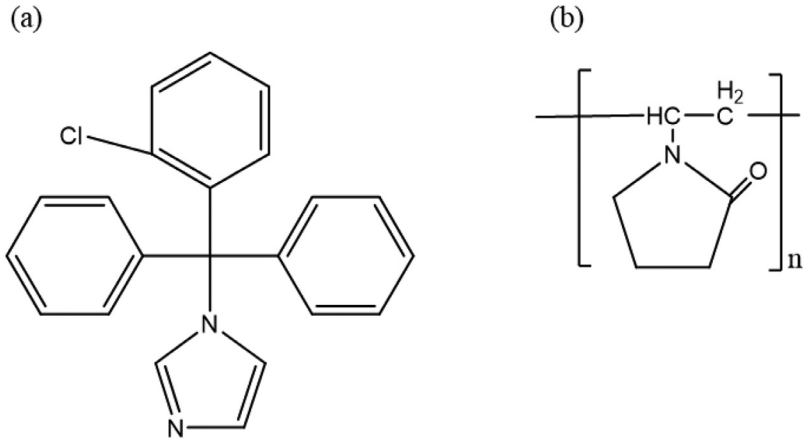

Fig. 1. Chemical structure for (a) clotrimazole and (b) PVP.

These nanoparticles were reported to significantly increase drug bioavailability,[6] possibly due to the reservoir[12] and particle drift[13-14] effects discussed in literature. Thus, congruent release may be the optimal release outcome for an ASD. For clarification of terminology, drug-rich nanoparticles with a glass transition below the experimental temperature are referred to as nanodroplets.

The issue with these formulations is that the benefits of congruent release are lost at higher drug loading, above the limit of congruency (LoC). This transition is sharp and results in a rapid decrease in release rate towards that of neat amorphous drug, an effect manifested as 'falling-off-the-cliff', which has been observed in PVP-, PVPVA-, and HPMC-based ASDs,[9,15] and to a lesser extent in HPMCAS-based ASDs.[16] The LoC is highly dependent on the drug-polymer system and has been observed to vary from 5% to 40% drug loadings.[15-18] Recent studies reported that drug-polymer interactions[18-19] and drug glass transition temperature[20] (T_g) can influence the LoC. Investigations revealed that ASDs can form a viscous surface gel layer[21-22] in the presence of water, a behavior often observed in neat polymer dissolution.[23-25] Physical phenomena arising from the subsequent thermodynamic incompatibility between drug and water were noted to have a complex effect on the erosion of the gel layer and, therefore, the release behavior of the ASD. Recent studies show that copovidone-based ASDs with low glass transition drugs form size-stable drug-rich nanodroplets in the gel layer when the drug loading is below the LoC, while a continuous drug-rich matrix forms in the gel layer at drug loadings above the LoC.[21,26-27] The latter acts as a drug-rich barrier at the surface of the ASD that inhibits release. This mechanism will herein be referred to as "Failure Mode II". A new failure mechanism, "Failure Mode I" will be introduced in the present study.

As indicated, the specific mechanisms that lead to a loss in congruent release have not been fully explored thus far. Our objective was to expand the list of known factors and failure modes that alter the LoC. In this study, we explored the effect of polymer molecular weight because it is a factor that strongly influences the properties of the gel layer and, therefore, could have implications for the LoC. We used poly(vinylpyrrolidone) (PVP) due to the wide variety of commercially available molecular weight grades. Clotrimazole was chosen as a model drug because it doesn't form strong interactions with PVP,[28] thus, it was used to minimize the confounding impact of drug-polymer interaction on LoC. In addition, clotrimazole is a slowly crystallizing drug. ASDs of clotrimazole were prepared with different polymers and at various drug loadings. Surface area normalized release studies were conducted to evaluate drug and polymer release rates in the absence of crystallization. Confocal fluorescence microscopy was used to study phase behavior at the ASD-solution interface. The results from this study provide additional insights into polymer selection for ASDs.

Materials

Clotrimazole (Fig. 1a) was obtained from Sigma-Aldrich (St. Louis, MO) and its melting point (141.2 °C ± 0.3), glass transition (28.0 °C ± 0.3), and amorphous solubility (10.3 μg/mL ± 0.6) were measured. In addition, the calculated pKa (6.26) and logP (5.84) were obtained from the Chemicalize software. Poly(vinylpyrrolidone) (PVP) grade K17, K25, K29/32, K60, and K90 were all received from Ashland Inc. (Covington, KY). PVP K12 was obtained from BASF (Ludwigshafen, Germany). The chemical structure of PVP is shown in Fig. 1b and the nominal molecular weight of each grade is tabulated in Table 1. Prodan was purchased from TCI America (Portland, OR). 1-propanol, iodine, and potassium iodide were bought from Sigma-Aldrich (St. Louis, MO). Deuterated dimethyl sulfoxide (DMSO) with tetramethylsilane (TMS) was acquired from Acros Organics (Geel, Belgium). Ethanol 200 proof was purchased from Decon Labs (King of Prussia, PA). HPLC grade acetonitrile and methanol; ACS grade citric acid, sodium phosphate monobasic monohydrate, and sodium phosphate dibasic anhydrous; and Alexa Fluor 488 NHS ester (succinimidyl ester) were purchased from Thermo Fisher Scientific (Waltham, MA).

Experimental methods

ASD powder preparation using rotary evaporation

Clotrimazole/PVP ASDs were prepared by solvent evaporation using a Heidolph Hei-VAP Core rotary evaporator (Heidolph Instruments, Schwabach, Germany) coupled to an Ecodyst EcoChyll S chiller (Ecodyst, Apex, NC). Drug and polymer were dissolved in ethanol in the desired drug:polymer ratio and the solvent was then removed under vacuum with a water bath temperature of 70 °C, rotation speed of 50–200 rpm, and chiller temperature of −30 °C, followed by heating to 80 °C and drying under vacuum for about 5 min. The resultant ASD was then further dried overnight under vacuum and at room temperature. Powder used to make the compacts that were subsequently imaged with fluorescence confocal microscopy also contained 0.1 and 0.003 wt.% of total solids of prodan and Alexa Fluor, respectively, which were added to ethanol prior to evaporation. PVP K60 comes as a 45% aqueous solution. 1-propanol was added to the solution to make a mixture at the azeotrope ratio of about 72:28 propanol-to-water. The azeotropic solution was

Table 1
Properties of PVP grades. Nominal weight average molecular weights (MW) were provided by the vendor.

PVP Grade	K12[a]	K17[a]	K25[a]	K29/32	K60	K90
MW ($g \cdot mol^{-1}$)	2500	10,000	34,000	58,000	400,000	1300,000
T_g Midpoint (°C)	101.5 ± 3.1	127.0 ± 2.2	–	177.3 ± 0.9	–	178.1 ± 0.1
c_e (v/v)	–	–	–	0.80	0.12	0.04
$d_T(c_e)$ (nm)	–	–	–	10	36	80
R_g (nm)	1	2	4	6	15	27
General Properties of PVP Molecular Chains						
$C_\infty = 14$[b]						
$M_0 = 111\ g \cdot mol^{-1}$						
$M_c = 46{,}620\ g \cdot mol^{-1}$						
$d_T = 8.7$ nm						

[a] Polymer chains are too short to entangle.
[b] Obtained from literature.[36]

evaporated as described previously, but at a water bath temperature of 80 °C. Residual water/solvent was removed by storing the material in an oven at 120 °C overnight and subsequently storing it at room temperature and under vacuum for another 12 h.

Glass transition and melting point

The glass transition (T_g) and melting point of samples were measured using a Q2000 differential scanning calorimeter (DSC) with a refrigerated cooling system (TA Instrument, New Castle, DE). The instrument baseline and temperature were calibrated according to the vendor instructions by using sapphire and indium samples, respectively. About 4–10 mg samples were weighed in Tzero aluminum pans and sealed with a hermetic lid. The lid was punctured to allow for complete drying. ASD and neat PVP samples were exposed to one drying cycle where they were heated to 110 °C, held for 30 min, and cooled to 25 °C. The samples were then exposed to either 3 or 4 heating and cooling cycles, where the heating and cooling ramp rates were 10 °C/min and the temperature range was between 25 and 200 °C. Crystalline clotrimazole samples were initially equilibrated to 50 °C, then with a heating and cooling rate of 10 °C/min, the samples were heated to 160 °C, cooled to −50 °C and then heated to 100 °C. All T_g values reported are from the midpoint of the glass transition range, determined at half height.

Amorphous solubility

Amorphous solubility was measured in pH 8.0, 50 mM phosphate buffer, which is at unionized conditions for clotrimazole, by using the UV extinction method.[11] Clotrimazole was dissolved in ethanol to 1.5 mg/mL and the solution was injected into 15 mL of pH 8.0 buffer at a 20 μL/min using a 3 mL syringe and 11 Elite syringe pump (Harvard Apparatus, Holliston, MA), while stirring at 300 rpm. The solution underwent liquid-liquid phase separation (LLPS) and formed drug-rich nanodroplets, since the solution concentration exceeded the amorphous solubility. These nanodroplets scatter light at wavelengths higher than the absorption wavelength. Thus, the amorphous solubility was determined by the onset of scattering light. A UV/vis spectrophotometer (SI Photonics, Tucson, Arizona), fitted with a dip probe was used to monitor transmission at 300 nm.

Dissolution of compact and quantification of release

The surface area of compacts was maintained throughout the release experiment by using a Woods intrinsic dissolution apparatus (Agilent, Santa Clara, CA). Powder was weighed into a flat, round die measuring approximately 0.8 cm in diameter and compressed at 1500 psi using a manual hydraulic press (Carver Inc., Wabash, IN) to prepare compacts with 0.5 cm^2 surface area. A dwell time of 1 min was used to allow for stress relaxation. The compact was left inside the die and the die was mounted to a stirring rod and submerged into 100 mL of pH 8.0, 50 mM phosphate buffer that was pre-equilibrated at 37 °C. At this pH, clotrimazole is largely unionized. ASD compacts were 100 mg in weight, while PVP compacts were 200 mg (250 mg for PVP K12) in weight. Compacts were rotated at 100 rpm and either 0.2 or 0.5 mL aliquots were sampled from the dissolution media and replaced with fresh media at set timepoints. The 0.2 mL aliquots were diluted to 0.5 mL with additional buffer. Aliquots of 3 mL were taken for samples containing PVP K12 and these were separated into 0.5 mL and 2.5 mL for drug and polymer analysis, respectively. The surface of any compact that did not fully release was scraped and inspected for the presence or absence of crystals using an Eclipse E200 polarized light microscope (PLM) (Nikon, Melville, NY).

All 0.5 mL samples were diluted with 0.5 mL of ethanol to dissolve the drug-rich nanodroplets and the concentration of solutes was measured using an 1100 Infinity high-performance liquid chromatography (HPLC) system (Agilent, Santa Clara, CA) with Agilent OpenLab CDS ChemStation software (version A.01.10.128) according to the parameters in Table S1. Clotrimazole was separated using an Ascentis Express C18 column (Sigma-Aldrich, St. Louis, MO) with dimensions of 10 cm x 3.0 mm, 2.7 μm bead size. All PVP grades, except K12, were separated using a size-exclusion A2500 column measuring 300 × 8 mm (MalvernPanalytical, Worcestershire, UK) and quantified according to the parameters in Table S1. This is because the molecular weight of PVP K12 was too low to be fully separated from the other buffer components with a size exclusion column. For PVP K12, the quantification method was adopted from literature.[29] By adding excess of iodine, a linear relationship between light absorbance at 500 nm and PVP concentration was obtained in the PVP concentration range of 5 to 40 μg/mL. The 2.5 mL samples were filtered using a 0.2 μm nylon syringe filter (Pall Corporation, Port Washington, NY) to remove the drug nanodroplets. The initial filtrate was discarded and only the last 0.8 mL of solution was collected. This was diluted to 5 mL by addition of 0.4 M citric acid so that the concentration fell into the range of the calibration curve. Then 1 mL of 0.006 N potassium triiodide reagent was added to the mixture, vortex mixed, and quickly transferred to a 1 cm cuvette. Light absorbance at 500 nm was measured with a UV–vis spectrophotometer (Varian Inc., Palo Alto, CA). The potassium triiodide reagent was prepared by dissolving 0.81 g of sublimed iodine and 1.44 g of potassium iodide in 1 L water.

In situ *imaging of compact*

Round, flat compacts with 0.5 cm^2 surface area were prepared as described above. ASD powder was prepared containing fluorescent dyes, prodan and Alexa Fluor 488, as discussed in the ASD preparation section. The 10% DL clotrimazole-PVP K12 ASD compact was

fused to the glass bottom of a dish well by heating to approximately 170 °C for 30 s while applying light pressure to the compact. Alternatively, the 10% DL clotrimazole-PVP K29/32 ASD compact was fused by using a brush to lightly coat the surface of the glass with methanol and immediately pressing the tablet on top. The methanol was then evaporated under vacuum for 1 hour. A round glass cover slip was placed on top of the compact. The experiment setup was described previously.[21]

The edge at the bottom of the compact was imaged with an A1Rsi confocal microscope (Nikon, Melville, NY) using the Nikon NIS-Elements AR software (version 5.20.01) every 30 s. The compact was submerged in 37 °C, pH 8.0, 50 mM buffer immediately after image collection started and a pipette was used to manually agitate the solution during imaging. Images were collected through a 60X, oil-immersion objective with a numerical aperture of 1.49 at 30 s intervals. Each image is a scan of 15 frames that were stitched with 10% overlap in a 15 × 1 horizontal grid. Each frame was collected in 260 milliseconds and contained 1024 × 1024 pixels with a pixel size of approximately 90 nm and an optical resolution of 230 nm. Prodan and Alexa Fluor 488 were excited at 409.0 and 488.0 nm and their emission were collected between 425 and 475 nm and 500–550 nm respectively. Note that regions labeled by Alex Fluor 488 and prodan in the images were digitally colored red and blue, respectively.

Nanodroplet composition measurement

Nanodroplets were prepared as follows. An ASD compact weighing approximately 200 mg was placed in a 4 mL vial and 300 μL of approximately 90 °C, pH 8.0, 50 mM phosphate buffer was added to it. The vial was capped and rotated at 100 rpm in a 90 °C water bath for 15 min to create an opaque nanodroplet suspension. The suspension was slowly cooled over approximately 10 min until it was warm to the touch. Roughly 100 μL samples were collected in triplicate centrifuged at 21,100 rcf and 37 °C for 15 min, using a Sorvall Legend Micro 21R centrifuge (Thermo Scientific, Waltham, MA). A portion of the pellet was inspected to confirm the absence of crystals using the PLM described above. The supernatant and pellet were sampled and dissolved in 0.7 mL dried, deuterated DMSO and 0.6 mL was transferred to a 5 mm tube for nuclear magnetic resonance (NMR) spectroscopy analysis.

Concentration analysis on the samples was performed using a Bruker Avance-III-800 spectrometer (Billerica, MA, USA) equipped with a QCI cryoprobe. ^{1}H spectra were collected at 25 °C over 4 scans with a repetition delay of 15 s. The chemical shift of the peaks was adjusted to that of tetramethylsilane (TMS) and the residual protonated DMSO (2.502 ppm) was used as a quantification reference. The singlet peaks of clotrimazole at 6.806 ppm and water at 3.321 ppm, as well as the broad band of peaks of PVP between 1.10 and 2.39 ppm were used to quantify the respective components based on measured standards and the concentrations were then converted to weight percent. Spectra were processed and analyzed using MestReNova software (Mestrelab Research, Santiago de Compostela, Spain) version 14.1.0–24,037.

ASD film preparation, exposure to relative humidity (RH), and imaging

Drug and polymer were dissolved in ethanol, such that the total solids concentration was 50 mg/mL. Prodan and Alexa Fluor 488 were added in concentrations of 0.1 and 0.003 wt.% of the total solids. About 5 μL of solution was spread on a glass slide and the ethanol was evaporated in a chamber filled with dry air. The films were further dried overnight at room temperature and under vacuum. Films were then placed in the headspace of a sealed jar containing purified and deionized water to create a relative humidity of 100%. The jar was placed in a 37 °C temperature-controlled oven. The films were removed from the chamber at different time intervals for imaging. Both exposed and fresh films were imaged. A closed chamber attached to an INU incubation system (Tokai Hit, Fujinomiya, Japan) was used to house the exposed films at 37 °C and 100% RH during the imaging process. The fluorescence confocal microscope described above was used to collect images with a resolution of 1024 × 1024 pixels in 2.7 s, through a 60x, oil-immersion objective with a numerical aperture of 1.49. Prodan and Alexa Fluor 488 were excited at 409.0 and 488.0 nm and their emissions were collected between 425 and 475 and 575–625 nm, respectively, using variable bandpass mode. Note that regions labeled by Alex Fluor 488 and prodan in the images were digitally colored red and blue, respectively.

Nanodroplet size measurement

Nanodroplet size was measured in a dilute environment using a Zetasizer Nano ZS dynamic light scattering (DLS) instrument and the Zetasizer software version 7.13 (Malvern Panalytical, Worcestershire, UK). Clotrimazole was dissolved in ethanol to make a 10 mg/mL stock solution. Then, 100 μL of stock solution was injected into 10 mL of 37 °C aqueous media over 10 s while mixing at 500 rpm using a stir bar. After injection was completed, about 2 mL of solution was transferred to a ZEN0040 cuvette (Malvern Panalytical, Worcestershire, UK) and placed in the Zetasizer at 37 °C. The size of the nanodroplets was acquired in the 173° backscatter mode over 15 measurements, each composed of one 30 s scan, with a 2 min delay.

Theory of polymer chain entanglements

Gel layer viscosity and diffusion of embedded particles/droplets are strongly affected by polymer chain entanglements. The ability of chains to entangle depends on their flexibility and length. For example, stiff and short chains cannot entangle. The critical size for a polymer chain to entangle can be estimated using the following relationship,[30]

$$M_c \approx 30 C_\infty M_0 \quad (1)$$

where M_c is the critical molecular weight needed for chains to entangle, C_∞ is a factor that describes the flexibility of the chains and is called the 'characteristic ratio', and M_0 is the monomer molecular weight. This was reported to be an accurate estimation in particular for vinyl polymers.[30] In addition to molecular weight and flexibility, chain entanglement also depends on polymer concentration. As polymer concentration increases in a solution, the individual polymer chains begin to overlap and then entangle. The critical polymer concentration needed for chains to entangle, c_e, can be calculated as,[31]

$$c_e = \frac{\rho M_c}{M_w} \quad (2)$$

where ρ is dry polymer density and M_w is the molecular weight of the polymer. Similarly, an entangled polymer matrix that is diluted by small molecules, such as drug or water, to below c_e will cause the polymer chains to become disentangled. The increase in viscosity originating from entangled polymer chains slows the diffusion of large particles according to the Stokes-Einstein relationship. These are particles that are larger than the reptation tube diameter, which is representative of the length between entangled points. However, particles smaller than the reptation tube diameter were observed to diffuse up to several orders of magnitude faster than predicted by the Stokes-Einstein relationship.[32-33] The reptation tube diameter can be estimated as,[30,34]

$$d_T = b\sqrt{\frac{M_c}{2M_0}} \quad (3)$$

where b is the statistical segment length and is roughly ~6 Å for the majority of linear polymers.[34-35] The reptation tube diameter

increases with dilution up to a maximum size at c_e given by,

$$d_T(c_e) = d_T c_e^{-\left(\frac{2}{3}\right)} \quad (4)$$

Lastly, the radius of gyration, R_g, of an unperturbed polymer chain can be estimated according to,[35]

$$R_g{}^2 = \frac{M_w b^2}{6M_0} \quad (5)$$

Results

Physicochemical properties of PVP

The glass transition of the various PVP grades initially increases with molecular weight, before reaching a similar value at high molecular weights, as shown in Table 1. The critical molecular weight for polymer chains to entangle, M_c, was estimated using Eq. (1) and the parameters listed in Table 1. An estimated M_c of 46,620 g/mol suggests that only PVP grades K29/32, K60, and K90 have polymer chains long enough to entangle. The distance between entangled points on the polymer chain is called the reptation tube diameter, d_T, and was estimated to be 8.7 nm for PVP (Table 1) by using Eq. (3) with a segment length of ~6 nm. When the polymer chains are diluted by small molecules (e.g. water or drug) d_T increases. Moreover, below a critical polymer concentration, c_e, the polymer chains cannot form entanglements. The value, c_e, was estimated with results shown in Table 1 for each PVP grade, using Eq. (2). The large molecular weight PVP K90 can form entanglements even when at a concentration of only 4% v/v, whereas the smaller PVP K29/32 can only form entanglements at a concentration of 80% v/v or above. The reptation tube diameter at this critical polymer concentration, $d_T(c_e)$, was also estimated in Table 1 by using Eq. (4). The reptation tube diameter has implications for the diffusion of embedded particles/droplets, which will be discussed later. In addition, the radius of gyration, R_g, was also estimated for PVP grades K29/32, K60, and K90 by using Eq. (5) and the results are listed in Table 1.

Release studies

The release profiles for neat PVP grades in buffer media are shown in Figure S5. The rate of release slowed with an increase in molecular weight. The ASD release profiles under nonsink conditions are shown in Fig. 2. The LoC of each ASD increased with an increase in PVP molecular weight. Furthermore, the apparent clotrimazole concentration analyzed from the dissolution media surpassed the neat clotrimazole amorphous solubility in all release experiments. Turbidity in the media was observed, which suggests that drug-rich nanodroplets formed. Congruently releasing systems were defined as those which released more than 80% of the drug and polymer from the ASD. PVP K12 and PVP K17 ASDs were incongruent even at a 5% drug loading, where polymer fully released but drug did not. ASDs with PVP K25 and higher molecular weight grades were able to fully release at low drug loading with congruent release, but not at high drug loading, where incongruent release was observed. Moreover, the release rate of congruently releasing ASDs showed a similar trend as for neat PVP, where ASDs with high molecular weight grades of PVP showed slower release rates of both drug and polymer.

Nanodroplet size stability in dilute suspensions

The size of clotrimazole nanodroplets was monitored over time in media with and without PVP. The diameter of the droplets at the initial timepoint was larger in the absence of polymer, however, it was not sensitive to polymer grade (Figure S6a). The droplets in buffer

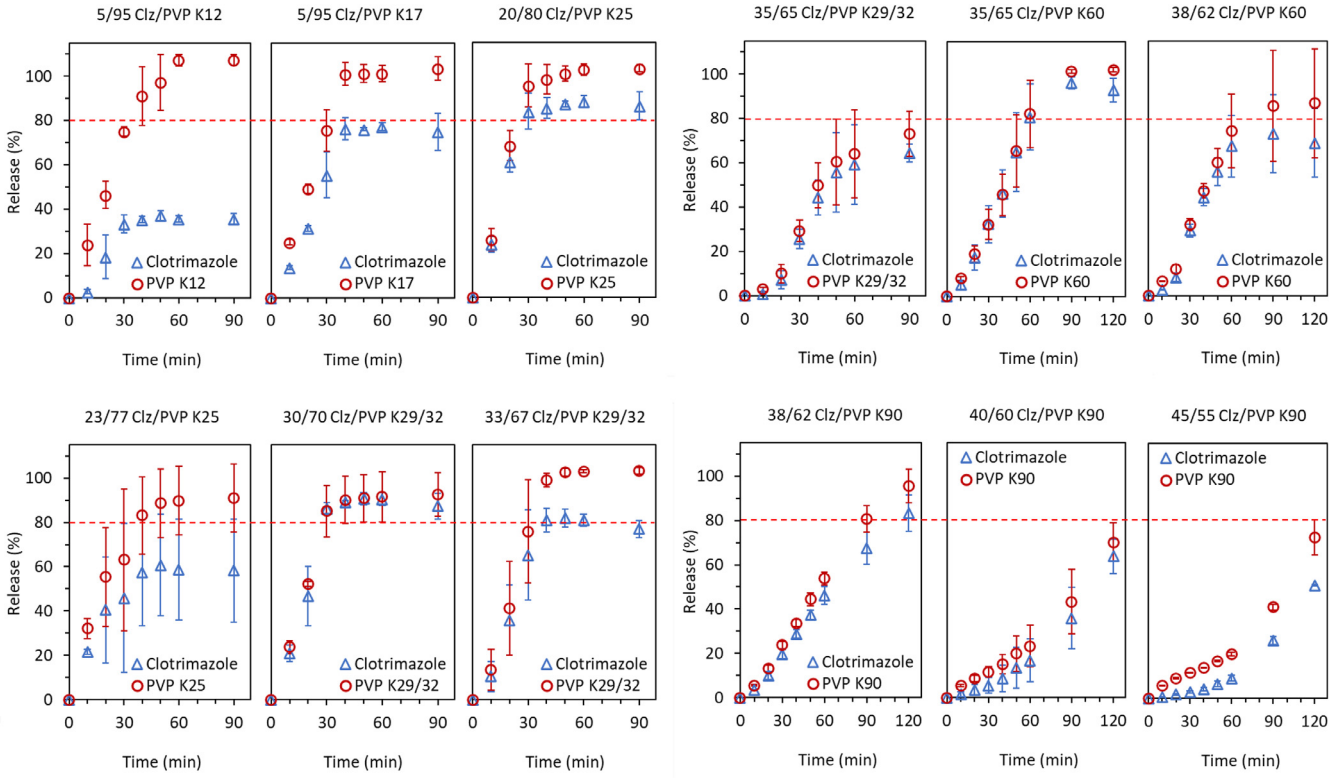

Fig. 2. Release profiles of clotrimazole and PVP from ASDs with different drug loading and PVP grades. Congruent releasing systems are those in which drug and polymer concentrations surpass the red dashed threshold. Error bars represent the standard deviations of $n = 3$.

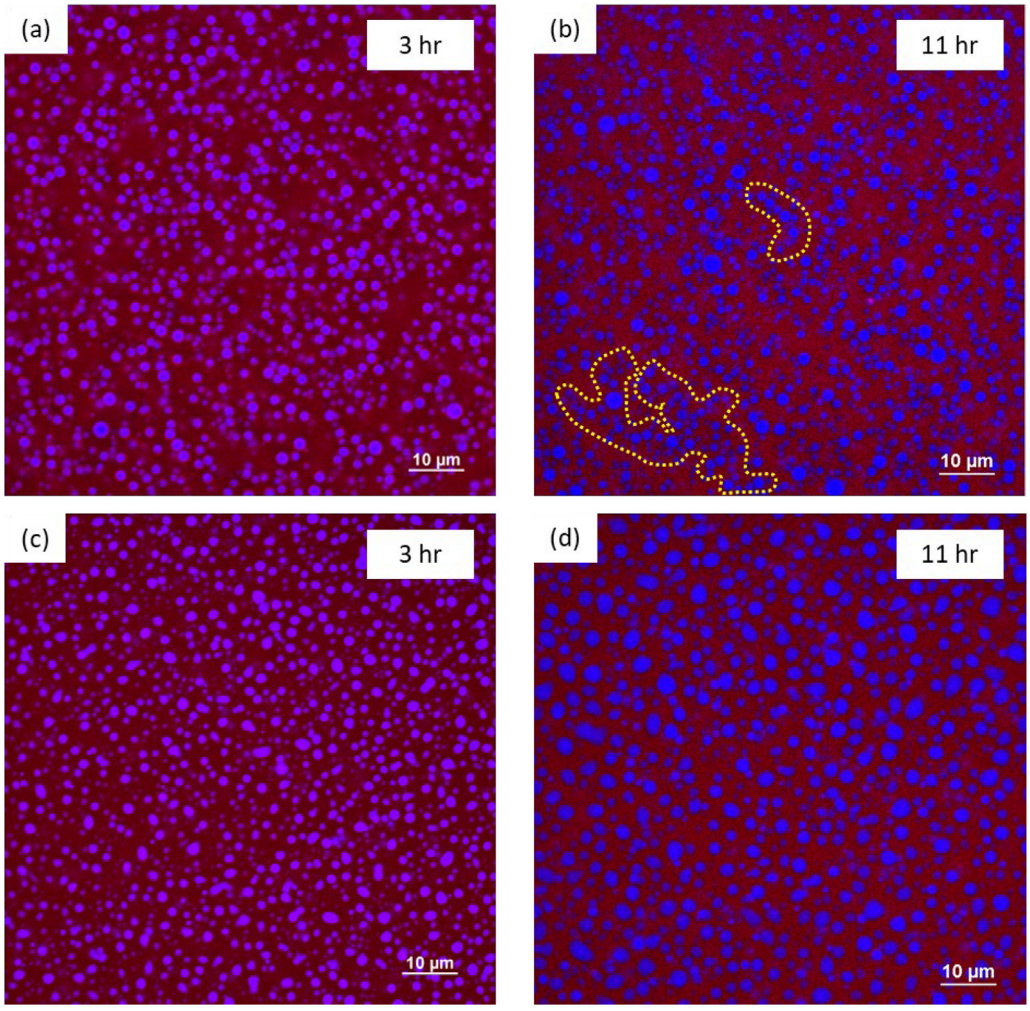

Fig. 3. ASD films exposed to 100% RH for 3 and 11 h, where panels (a) and (b) represent 10% DL clotrimazole-PVP K12 films and panels (c) and (d) represent 10% DL clotrimazole-PVP K29/32 films. Yellow dotted outlines highlight examples of droplets clustering into strands.

had an initial diameter of ~540 nm and grew to ~1 μm. In comparison, the initial size was ~340 and ~290 nm and grew to ~610 and ~630 nm in the presence of 1 mg/mL PVP K12 and PVP K29/32, respectively. Despite the difference in size, the rate of growth was similar across all 3 media, as shown by the normalized diameter in Figure S6b. The results suggest that clotrimazole nanodroplets are unstable and PVP is not a good stabilizer in dilute suspensions, even at a high polymer-to-drug weight ratio of 10:1.

Phase behavior of ASD films exposed to high relative humidity

ASD films labeled with fluorophores and composed of 10% DL clotrimazole-PVP K12 and 10% DL clotrimazole-PVP K29/32 had a uniform magenta color, suggesting the drug and polymer were homogeneously distributed (Figure S4). Phase separation was observed after exposure to 100% RH for 3 h (Fig. 3). The blue and red regions represent the drug-rich hydrophobic and water/polymer-rich hydrophilic phases containing prodan and Alexa Fluor 488, respectively. The drug-rich phase appeared as droplets, while the hydrophilic phase was continuous for both ASD films. However, the distribution pattern of the droplets differed. Qualitatively, the drug-rich domains appeared to extensively agglomerate into strands in the PVP K12 ASD film, especially after 11 h of exposure (Fig. 3b). This agglomeration behavior is likely the mechanism behind the poor release of this system and is herein referred to as "Failure Mode I". Failure Mode I was not observed for the PVP K29/32 ASD films, as the droplets were stable (Fig. 3d).

Films above 10% DL were also exposed to 100% RH for 1 h and imaged as shown in Fig. 4. The drug-rich phase formed as droplet domains for up to 30% DL. However, a significant change in behavior was observed as drug loading increased to 40%. At 40% DL, the drug-rich phase manifested as a continuous phase, instead of droplets. At the same time, the hydrophilic phase appeared as dispersed droplets within the drug-rich matrix. This behavior is widely known as phase inversion and it has been shown to be a failure mode for ASD release in other systems as well.[21,26-27] Herein, it is referred to as "Failure Mode II". Interestingly, the clotrimazole-PVP K12 ASD system is limited by Failure Mode I at <5% drug loading, but it also exhibits Failure Mode II between 30 and 40% drug loading. If Failure Mode I were to be prevented, then the LoC would have been limited by Failure Mode II.

Phase behavior of ASD compacts in contact with buffer

ASD compacts containing 10% DL clotrimazole-PVP K12 and 10% DL clotrimazole-PVP K29/32 were used to study the phase behavior at the ASD/solution interface during release. The compacts were labeled with the same fluorescent probes as the films. Prior to exposure to buffer, prodan and Alexa Fluor 488 were uniformly distributed in the compact, indicating the homogeneity of the ASD

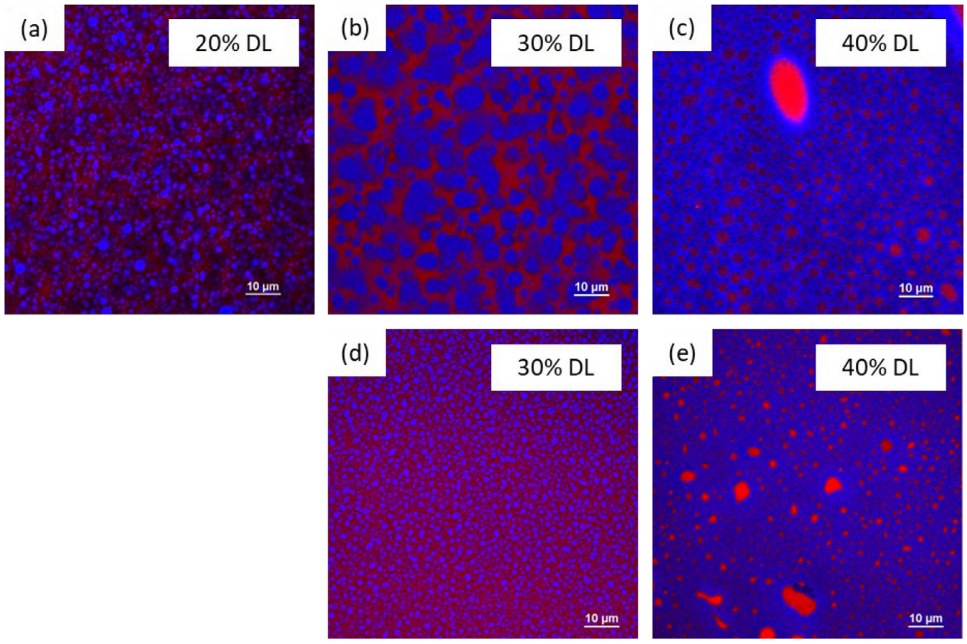

Fig. 4. ASD films exposed to 100% RH for 1 hour, where panels (a), (b), and (c) represent clotrimazole-PVP K12 films and panels (d) and (e) represent clotrimazole-PVP K29/32 films.

(Figure S1). Once exposed to buffer, water rapidly penetrated the dry ASD to form a gel layer in which phase separation was detected through the segregation of the dyes. Cross sectional snapshots of the compacts were taken at 2 min and after more than 7 min for the PVP K12 and PVP K29/32 ASDs, respectively, as shown in Fig. 5. Water penetrated into the compact from right to left. The darker region on the right, labeled "3", is the solution phase. Region "2" is the gel layer (i.e. hydrated ASD) and region "1" is dry ASD. The pattern of behavior in the phase separated region of the gel layer differed between the two ASDs. The PVP K12 ASD exhibited significant nanodroplet agglomeration after a certain point in the gel layer (Fig. 5a). The nanodroplets arranged in a strand-like morphology, which resulted in an interconnected network of droplets. As the hydrophilic phase surrounding these connected droplets was further diluted and the

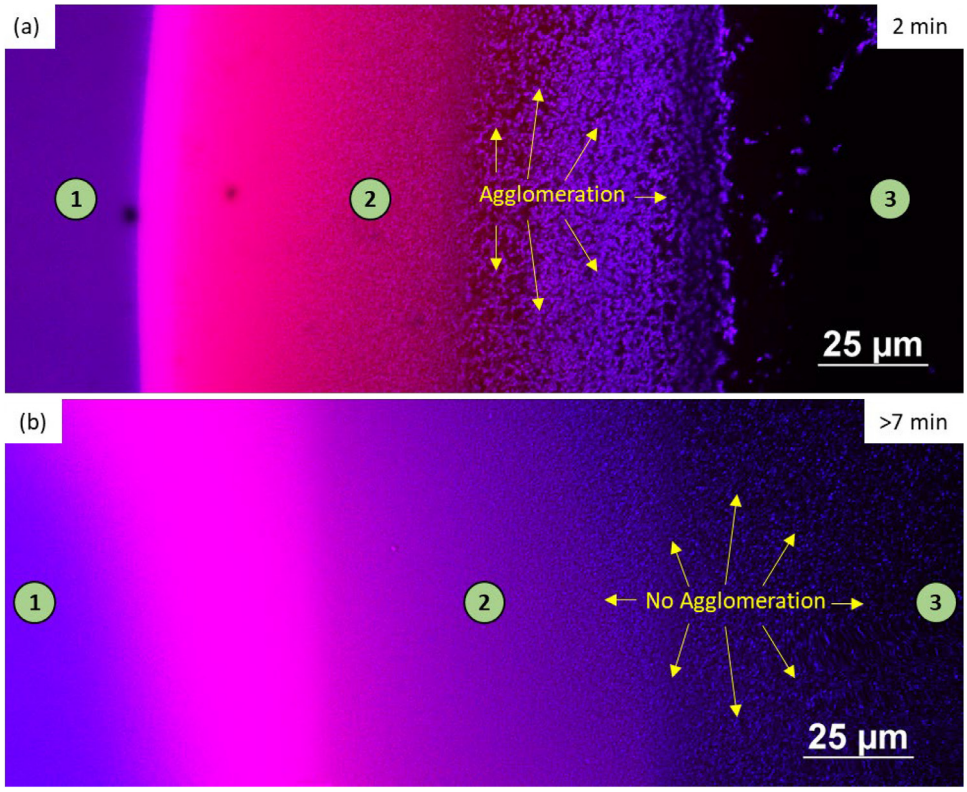

Fig. 5. In situ fluorescence confocal microscope images at the ASD dissolution front for (a) 10% DL clotrimazole-PVP K12 ASD after 2 min of dissolution and (b) 10% DL clotrimazole-PVP K29/32 ASD after more than 7 min of dissolution. The green circles refer to dry ASD (1), gel layer (2), and solution (3).

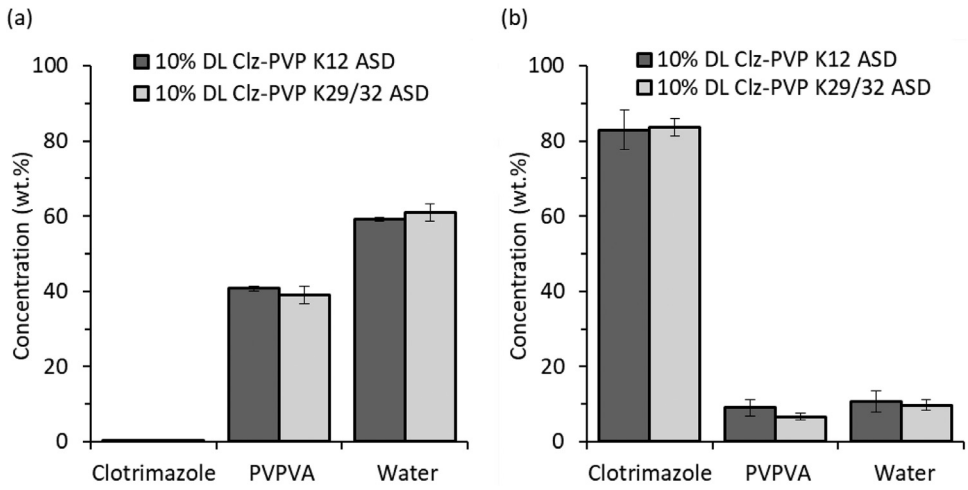

Fig. 6. Composition of hydrophilic (a) and hydrophobic (b) phases resulting from a 40:60 mixture of ASD-to-water. Error bars represent the standard deviations of $n = 4$. Clz stands for clotrimazole.

polymer diffused out, it caused the network to collapse and form denser agglomerated regions closer to the solution phase, which prevented these drug-rich nanodroplets from releasing. As mentioned previously, this is Failure Mode I for release, which leads to a low LoC. This process continued over time (Figure S2). In contrast, the PVP K29/32 ASD did not show nanodroplet agglomeration in the gel layer or after they were released into the solution phase (Fig. 5b and Figure S3).

Composition of nanodroplets in concentrated suspensions

The compositions of the hydrophilic phase (i.e. solution) and hydrophobic phase (i.e. nanodroplets) were studied in concentrated suspensions by mixing an ASD and water in a 40:60 ratio to more closely represent the gel layer environment during ASD release. The two ASDs studied were 10% DL clotrimazole-PVP K12 and 10% DL clotrimazole PVP K29/32. Statistically, the composition of the phases between the two systems were similar, as shown in Fig. 6. This suggests that polymer molecular weight did not have a significant effect on the thermodynamics of the system. PVP preferred to segregate from clotrimazole during water-induced phase separation. The hydrophobic phase was drug-rich with about ~80 wt.% clotrimazole, whereas the hydrophilic phase was rich in PVP (~40 wt.%) and water (~60 wt.%) and contained only trace amounts of clotrimazole. This behavior has been termed segregative phase separation[37-39] and it occurs in weakly interacting drug-polymer systems. In strongly interacting drug-polymer systems the phase separation is associative[37-38] and the polymer prefers to distribute more in the hydrophobic phase relative to in the hydrophilic phase.[39]

Discussion

As more new molecular entities with low aqueous solubility are being advanced into clinical development, the industry is relying more on ASDs as a formulation strategy to improve drug bioavailability. Not only do ASDs result in faster release rates compared to their crystalline counterparts, but they also lead to the formation of drug-rich nanodroplets in certain cases. These nanodroplets act as a fast-replenishing drug reservoir and have been proven beneficial for drug absorption.[5,7,40] Thus, the optimal release outcome for ASD formulations is to generate a drug concentration that exceeds the amorphous solubility and form drug-rich nanodroplets which can maintain a maximum free drug concentration for a sustained period of time during absorption. Previous studies have shown that this optimum outcome can only be achieved when polymer and drug release congruently (i.e. at the same rate).

Congruent release

In the congruent release regimen of ASDs, release is dictated by the polymer, which results in a drug release rate much faster than from neat amorphous drug.[8] For example, the release rate of clotrimazole from congruently releasing PVP-based ASDs (Fig. 2) is similar to the release rate of the neat PVP (Figure S5). This is because the release mechanism of ASDs is similar to that of neat glassy polymers.[21,27,41] The process begins with water penetration into the glass, which causes it to transition to a viscous rubbery state (i.e. a gel layer). This glass-gel boundary was observed as a sharp color transition on the left side of the images in Fig. 5 (between regions 1 and 2). The penetration of water develops concentration and viscosity gradients across the gel layer and the solution diffusion boundary layer as depicted in Figure S7. The viscosity gradient in the gel layer is higher than that of the diffusion boundary layer of the solution. At the end of the gel layer, the viscosity is low enough for the polymer chains to be able to release into the solution (gel-solution boundary). At this point any droplets or solutes, such as dye, that were initially trapped in the high viscosity gradient of the gel layer are also able to release into solution. Hence, the gel-solution boundary is where the red fluorescence signal drops to background (black, between regions 2 and 3) in Fig. 5. The high viscosity in the gel layer is caused by the low translational diffusion of polymer chains as they overlap and, in some cases (K29/32, K60, and K90), entangle with each other due to their large size.

In many cases, ASDs exhibit a miscibility gap in the gel layer due to water ingress, which results in phase separation. Water-rich hydrophilic and amorphous drug-rich hydrophobic phases are formed in this process. During congruent release (Fig. 5b), the hydrophobic phase forms as stable nanodroplets that are dispersed, and remain dispersed, in the hydrophilic phase. Since the polymer is hydrophilic, it often partitions mostly into the hydrophilic phase (Fig. 6), although not always.[26,39,42-44] Thus, the drug-rich nanodroplets are initially trapped in the viscous hydrophilic phase until the gel transitions to a solution (Fig. 5b). At this transition, the drug-rich nanodroplets are released into solution along with the polymer chains and this process continues until all of the ASD releases, remarkably, even in non-sink conditions (Fig. 2). In summary, the kinetics of drug release from congruent releasing ASDs are limited by

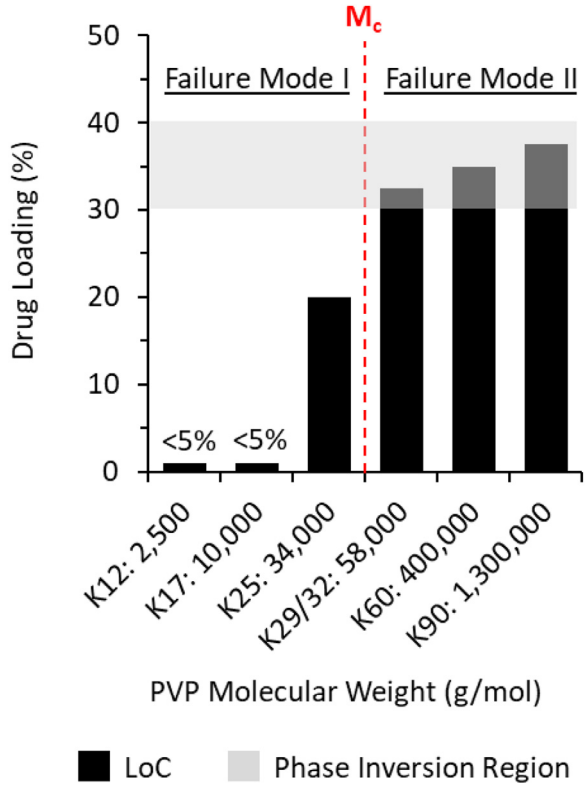

Fig. 7. Effect of PVP molecular weight on the limit of congruency for clotrimazole-PVP ASDs. M_c is the critical molecular weight for entanglement from Table 1. The phase inversion range for K17, K25, K60, and K90 was inferred based on data from K12 and K29/32.

water penetration into the glass and subsequent release of polymer chains into solution.

Limit of congruency and loss of drug release

At higher drug loadings, the polymer has little influence over the release of drug from the ASDs,[8] whereby drug and polymer often release at independent rates (i.e. incongruent). This was observed for ≥5% DL PVP K12, ≥5% DL PVP K17, ≥23% DL PVP K25, ≥35% DL PVP K29/32, and ≥45% DL PVP K90. In addition, a loss in polymer-driven release results in poor and incomplete drug release (<80% in Fig. 2). The maximum drug loading where the system maintains congruent release is termed the limit of congruency (LoC). Since the variability in the experiments made it difficult to detect incongruent release in certain cases (e.g. 35% DL PVP K29/32, 38% DL PVP K60, and 40% DL PVP K90 ASDs in Fig. 2), LoC was defined as the highest drug loading in which drug release exceeded 80%. The polymer molecular weight had a surprising effect on LoC. As shown in Fig. 7, the LoC was below 5% at low molecular weights (e.g. PVP K12 and K17). However, when the molecular weight of the polymer increased across a narrow threshold, the LoC rapidly increased to over 30% drug loading. This molecular weight threshold is close to where polymer chains are expected to entangle (M_c). Further increases in LoC were minimal above this molecular weight.

Failure modes leading to poor release

Nanodroplet agglomeration (Failure mode I)

The lower LoC values observed for PVP molecular weights below M_c (K12, K17, and K25) appears to be caused by nanodroplet agglomeration in the gel layer (Figs. 3a,b and 5a). This is a newly discovered and distinctly different mechanism than the phase inversion process that was presented in previous studies.[21,26] The failure mode as a function of PVP molecular weight is summarized in Fig. 7. We have termed the agglomeration mechanism as Failure Mode I and the phase inversion mechanism as Failure Mode II to differentiate their effect on the LoC. The nanodroplets formed in the gel layer appear initially dispersed, as shown in the micrographs of the 10% DL PVP K12 compacts exposed to buffer (Fig. 5a). However, the droplets agglomerated closer to the gel/solution boundary, forming an interconnected network of strings. This nanodroplet network was anchored into the gel layer and had enough strength to withstand the hydrodynamic forces. Therefore, the drug-rich nanodroplets accumulated at the gel-solution interface and did not release into solution. This extent of droplet agglomeration was not observed for the ASD with PVP K29/32 (Fig. 3c,d and 5b).

Phase inversion (Failure mode II)

Previous studies show that congruency can be lost when the phase separation morphology changes in the gel layer. Congruent release occurs if the hydrophobic phase forms as dispersed nanodroplets, which remain dispersed throughout the release process. However, when drug loading is increased, the relative volume of the hydrophobic phase increases accordingly. Above a certain relative volume, the morphology of the phases inverts, where the hydrophobic phase develops as a continuous domain and the hydrophilic phase forms as dispersed domains.[21,27] A continuous hydrophobic phase cannot be physically released into solution, because it is anchored into the high viscosity gel layer. Moreover, its presence on the surface acts as a barrier to further water penetration. Phase inversion would occur at a different drug loading if the composition of the hydrophobic phase differed between the systems studied. However, this was not the case for the grades of PVP and clotrimazole as shown in Fig. 6. Indeed, direct observations of phase inversion (Fig. 4) confirm that phase inversion occurs between 30 and 40% DL for ASDs with both K12 and K29/32, suggesting that for this system polymer molecular weight does not appear to influence the phase inversion. As a corollary, the LoC for ASDs with K29/32, and possibly K60 and K90, is limited by phase inversion (Failure Mode II), as observed for other drug-polymer systems.[21,26-27] However, this was not the case for K12, K17, and K25, because the LoC for these systems is significantly below the drug loading needed for phase inversion, as illustrated in Fig. 7. In summary, it appears that there are two independent mechanisms that lead to the limit of congruency and loss of release, and these are influenced by the molecular weight of the polymer for the clotrimazole-PVP system. When PVP molecular weight is below the estimated critical size for chain entanglement (M_c) a lower LoC results due to extensive nanodroplet agglomeration in the gel layer (Failure Mode I). However, this agglomeration behavior is inhibited at molecular weights above M_c, at which point the LoC is limited by the drug loading where phase inversion occurs (Failure Mode II).

Role of polymer molecular weight on preventing nanodroplet agglomeration

The exact mechanism behind the effect of high molecular weight on the inhibition of droplet agglomeration for the clotrimazole-PVP system has not been fully elucidated. Nevertheless, we provide possible hypotheses for this observed behavior. Initially we thought that one possibility was for polymer to adsorb at the nanodroplet surface and prevent droplets from agglomerating through steric repulsion of polymer chains, where larger molecular weight polymer chains are expected to provide better nanodroplet stability due to stronger steric repulsion.[45-47] However, Figure S6 shows that neither PVP K29/32 nor PVP K12 had an effect on the growth rate of the nanodroplets in dilute solution, so we expect that stabilization through steric

repulsion is not the likely mechanism leading to stable nanodroplets in the ASD gel layer for PVP K29/32 or higher molecular weight grades.

However, larger molecular weight polymer chains are also known to entangle due to their long chain length, whereby the diffusion of embedded molecules and particles in the polymeric matrix can be greatly affected. The observation that the increase in LoC occurs near the estimated critical molecular weight where chains entangle (M_c) gives support to the hypothesis that polymer chain entanglement may be contributing to the stabilization of the nanodroplets in Figs. 3c,d and 5b. When polymer chains entangle, the viscosity increases sharply.[48] However, the viscous resistance that molecules and droplets exhibit in the gel layer can be greatly affected by their size. Droplets and molecules much smaller than the distance between entanglements, d_T, do not experience the viscous effects which arise from chain entanglement.[32-33] In other words, they diffuse as if no entanglements are present and only the local viscosity created from the friction of the polymer chains affects their mobility. This is the case for water and individual drug molecules. In contrast, droplets much larger than d_T are restricted by the entangled chains and their diffusion rate is slowed considerably, as illustrated in Figure S8. Thus, the entangled chains can be thought of as a "fishnet", where droplets smaller than the gap in the netting "fall through" and larger droplets get "captured" in the netting. The clotrimazole-rich nanodroplets are a few hundred nanometers in diameter (Figure S6 and Fig. 5), while the maximum d_T calculated is 80 nm for PVP K90 at the disentanglement concentration (Table 1), so the droplets are too large to pass through this polymer "fishnet". In addition, entangled polymers swell more in the presence of solvent, yielding a considerably thicker gel layer.[24] The swelling process is expected to increase the distance between the nanodroplets. However, during this swelling process, the polymer chains are getting diluted and the distance between them increases, which eventually leads to them disentangling. When the polymer chains eventually disentangle, the droplets are sufficiently apart to not immediately agglomerate. In the case of PVP K29/32, the polymer chains are expected to become disentangled when the polymer volume fraction is at or below 0.8 (Table 1), which explains why there was no observed stabilization in dilute solution (Figure S6). In contrast, low molecular weight PVP, such as K12, is too short to entangle and form a "fishnet" for the nanodroplets (Figure S8). The consequence is that the nanodroplets become prone to agglomeration (Figs. 3a,b and 5a).

Implications for ASD formulation design

These failure modes add to the list of considerations when designing a formulation. From the clotrimazole-PVP ASD system it appears that Failure Mode I occurs at lower drug loadings than Failure Mode II. This is conceptually expected because at drug loadings above Failure Mode II the system cannot generate nanodroplets. The clotrimazole-PVP ASD system is a non-interacting drug-polymer ASD where the drug-rich nanodroplets have a low T_g, so Failure Mode II occurred at moderate drug loadings. However, for highly interacting drug-polymer systems it's been shown that Failure Mode II can occur at drug loadings as low as 5–10%.[21,26] If a different polymer or additive were added to increase the drug loading where Failure Mode II occurs, then it's possible that the new system may become limited by Failure Mode I. A holistic approach to formulation development should consider both mechanisms.

To prevent Failure Mode I, it is best to avoid scenarios which promote nanodroplet agglomeration. These scenarios may be contrary to what has been thought necessary to improve a formulation. For example, reducing nanodroplet size is generally considered an improvement for bioavailability, however, size reduction can also make the nanodroplets more unstable and increases the risk of Failure Mode I. In polymer-controlled ASD release, low molecular weight polymer yields faster drug release, however, it can also trigger Failure Mode I. Additives, such as surfactants, can lower the T_g of the system and reduce the physical stability of the ASD. Nevertheless, they can also stabilize the nanodroplets and may prevent Failure Mode I. Lastly, partially ionized nanodroplet surfaces can also increase their stability, so the pK_a of the drug and pH of the media are also important considerations for preventing Failure Mode I.

A distinctly different approach must be taken for Failure Mode II. This has been extensively covered in a previous publication.[21,26] First, phase inversion will always occur in unionized conditions as drug loading is increased, but steps can be taken to increase the drug loading at which this occurs. Failure Mode II is primarily driven by the thermodynamics of the system, therefore, drug-polymer-water interactions play a crucial role in dictating the drug loading where Failure Mode II occurs for a specific drug-polymer ASD system. Different polymer and additive chemistry should be evaluated to optimize against Failure Mode II. It has also been noted that strong drug-polymer interactions trigger Failure Mode II at lower drug loads. Since strong drug-polymer interactions are preferable for achieving robust physical stability on storage, the ASD system has to be balanced.

Conclusion

The results in this study highlight that there is more than one mechanism underlying the LoC phenomenon. Previous studies showed that the polymer in the ASD causes a gel layer to form when in contact with dissolution media. Furthermore, the water in the gel layer induces phase separation, which results in the formation of a drug-rich hydrophobic phase and a water/polymer-rich hydrophilic phase. The morphology of phase separation controls the subsequent release behavior, where dispersed hydrophobic domains lead to congruent release and continuous domains lead to incongruent release. The change in morphology from a dispersed to a continuous phase is called phase inversion (Failure Mode II) and the drug loading needed for phase inversion was reported to depend on drug-polymer interaction strength. In this study, fluorescence confocal microscopy was used to show that instability of the initially dispersed hydrophobic domains, leading to droplet agglomeration in the gel layer (Failure Mode I), can also result in incongruent release. This newly investigated mechanism leads to a lower LoC than would be anticipated by considering the drug loading where phase inversion occurs. By stabilizing the dispersed hydrophobic domains with higher molecular weight PVP, the LoC increased from less than 5% to over 30%. Theoretical considerations suggest that the high MW polymer chains are entangled, stabilizing the drug-rich nanodroplets in the gel layer against agglomeration by hindering their translational diffusion and increasing their separation distance through swelling. This study highlights the need to identify the mechanisms underlying the LoC phenomenon in order to improve drug loading limits in ASDs and ultimately maximize the bioavailability of ASDs.

Declaration of competing interest

The authors declare the following financial interests/personal relationships which may be considered as potential competing interests: AbbVie and Purdue University jointly participated in study design, research, data collection, analysis and interpretation of data, writing, reviewing, and approving the publication. A.D., C.Q., and M.L. C. have no additional conflicts of interest to report. A.S.I. and Y.G. are, and G.G.Z.Z. was, employees of AbbVie and may own AbbVie stock. L. S.T is an Editorial Board Member of the Journal of Pharmaceutical Sciences and Editor-in-Chief of Molecular Pharmaceutics and was not involved in the editorial review or the decision to publish this article.

Acknowledgements

The authors would like to thank AbbVie Inc. and the Center for Bioanalytic Metrology (CBM), for their financial support.

Supplementary materials

Supplementary material associated with this article can be found in the online version at doi:10.1016/j.xphs.2024.10.026.

References

1. He Y, Ho C. Amorphous solid dispersions: utilization and challenges in drug discovery and development. *J Pharm Sci*. 2015;104(10):3237–3258.
2. Tan DK, Davis DA, Miller DA, Williams RO, Nokhodchi A. Innovations in thermal processing: hot-melt extrusion and KinetiSol® dispersing. *AAPS PharmSciTech*. 2020;21(8):1–20.
3. Agarwal P, Huckle J, Newman J, Reid DL. Trends in small molecule drug properties: a developability molecule assessment perspective. *Drug Discov Today*. 2022 103366.
4. Taylor LS, Zhang GGZ. Physical chemistry of supersaturated solutions and implications for oral absorption. *Adv Drug Deliv Rev*. 2016;101:122–142.
5. Wilson V, Lou X, Osterling DJ, et al. Relationship between amorphous solid dispersion in vivo absorption and in vitro dissolution: phase behavior during dissolution, speciation, and membrane mass transport. *J Control Release*. 2018;292:172–182.
6. Kesisoglou F, Wang M, Galipeau K, Harmon P, Okoh G, Xu W. Effect of amorphous nanoparticle size on bioavailability of anacetrapib in dogs. *J Pharm Sci*. 2019;108 (9):2917–2925.
7. Stewart AM, Grass ME, Brodeur TJ, et al. Impact of Drug-Rich Colloids of Itraconazole and HPMCAS on Membrane Flux in Vitro and Oral Bioavailability in Rats. *Mol Pharm*. 2017;14(7):2437–2449.
8. Indulkar AS, Lou X, Zhang GGZ, Taylor LS. Insights into the dissolution mechanism of ritonavir–copovidone amorphous solid dispersions: importance of congruent release for enhanced performance. *Mol Pharm*. 2019;16(3):1327–1339.
9. Que C, Lou X, Zemlyanov DY, et al. Insights into the dissolution behavior of ledipasvir–copovidone amorphous solid dispersions: role of drug loading and intermolecular interactions. *Mol Pharm*. 2019;16(12):5054–5067.
10. Saboo S, Mugheirbi NA, Zemlyanov DY, Kestur US, Taylor LS. Congruent release of drug and polymer: a “sweet spot” in the dissolution of amorphous solid dispersions. *J Control Release*. 2019;298:68–82.
11. Ilevbare GA, Taylor LS. Liquid–liquid phase separation in highly supersaturated aqueous solutions of poorly water-soluble drugs: implications for solubility enhancing formulations. *Cryst Growth Des*. 2013;13(4):1497–1509.
12. Indulkar AS, Gao Y, Raina SA, Zhang GGZ, Taylor LS. Exploiting the phenomenon of liquid–liquid phase separation for enhanced and sustained membrane transport of a poorly water-soluble drug. *Mol Pharm*. 2016;13(6):2059–2069.
13. Sugano K. Possible reduction of effective thickness of intestinal unstirred water layer by particle drifting effect. *Int J Pharm*. 2010;387(1–2):103–109.
14. Narula A, Sabra R, Li N. Mechanisms and extent of enhanced passive permeation by colloidal drug particles. *Mol Pharm*. 2022;19(9):3085–3099.
15. Saboo S, Moseson DE, Kestur US, Taylor LS. Patterns of drug release as a function of drug loading from amorphous solid dispersions: a comparison of five different polymers. *Eur J Pharm Sci*. 2020;155: 105514.
16. Yang R, Mann AK, Van Duong T, et al. Drug release and nanodroplet formation from amorphous solid dispersions: insight into the roles of drug physicochemical properties and polymer selection. *Mol Pharm*. 2021;18(5):2066–2081.
17. Hiew TN, Zemlyanov DY, Taylor LS. Balancing solid-state stability and dissolution performance of lumefantrine amorphous solid dispersions: the role of polymer choice and drug–polymer interactions. *Mol Pharm*. 2021;19(2):392–413.
18. Que C, Deac A, Zemlyanov DY, et al. Impact of drug–polymer intermolecular interactions on dissolution performance of copovidone-based amorphous solid dispersions. *Mol Pharm*. 2021;18(9):3496–3508.
19. Saboo S, Kestur US, Flaherty DP, Taylor LS. Congruent release of drug and polymer from amorphous solid dispersions: insights into the role of drug-polymer hydrogen bonding, surface crystallization, and glass transition. *Mol Pharm*. 2020;17 (4):1261–1275.
20. Hiew TN, Taylor LS. Combining drug salt formation with amorphous solid dispersions—a double edged sword. *J Control Release*. 2022;352:47–60.
21. Deac A, Qi Q, Indulkar AS, Gao Y, Zhang GGZ, Taylor LS. Dissolution mechanisms of amorphous solid dispersions: a close look at the dissolution interface. *Mol Pharm*. 2023;20(4):2217–2234.
22. Han YR, Ma Y, Lee PI. Impact of phase separation morphology on release mechanism of amorphous solid dispersions. *Eur J Pharm Sci*. 2019;136: 104955.
23. Ueberreiter K, Asmussen F. Velocity of dissolution of polymers. *Part I J Polym Sci*. 1962;57(165):187–198.
24. Papanu JS, Soane DS, Bell AT, Hess DW. Transport models for swelling and dissolution of thin polymer films. *J Appl Polym Sci*. 1989;38(5):859–885.
25. Miller-Chou BA, Koenig JL. A review of polymer dissolution. *Prog Polym Sci*. 2003;28(8):1223–1270.
26. Deac A, Luebbert C, Qi Q, et al. Dissolution mechanisms of amorphous solid dispersions: application of ternary phase diagrams to explain release behavior. *Mol Pharm*. 2024;21(4):1900–1918.
27. Yang R, Zhang GGZ, Zemlyanov DY, Purohit HS, Taylor LS. Release mechanisms of amorphous solid dispersions: role of drug-polymer phase separation and morphology. *J Pharm Sci*. 2023;112(1):304–317.
28. Que C, Qi Q, Zemlyanov DY, et al. Evidence for halogen bonding in amorphous solid dispersions. *Cryst Growth Des*. 2020;20(5):3224–3235.
29. Levy GB, Fergus D. Microdetermination of polyvinylpyrrolidone in aqueous solution and in body fluids. *Anal Chem*. 1953;25(9):1408–1410.
30. Wool RP. Polymer entanglements. *Macromolecules*. 1993;26(7):1564–1569.
31. Graessley WW. Polymer chain dimensions and the dependence of viscoelastic properties on concentration, molecular weight and solvent power. *Polymer (Guildf)*. 1980;21(3):258–262.
32. Tuteja A, Mackay ME, Narayanan S, Asokan S, Wong MS. Breakdown of the continuum Stokes– Einstein relation for nanoparticle diffusion. *Nano Lett*. 2007;7 (5):1276–1281.
33. Yamamoto U, Schweizer KS. Theory of nanoparticle diffusion in unentangled and entangled polymer melts. *J Chem Phys*. 2011;135(22): 224902.
34. Milner S. Predicting the tube diameter in melts and solutions. *Macromolecules*. 2005;38(11):4929–4939.
35. Hiemenz PC, Lodge TP. *Polymer Chemistry*. CRC press; 2007.
36. Tarazona MP, Saiz E. Combination of SEC/MALS experimental procedures and theoretical analysis for studying the solution properties of macromolecules. *J Biochem Biophys Methods*. 2003;56(1–3):95–116.
37. Minton AP. Simple calculation of phase diagrams for liquid–liquid phase separation in solutions of two macromolecular solute species. *J Phys Chem B*. 2020;124 (12):2363–2370.
38. Spruijt E, Westphal AH, Borst JW, Cohen Stuart MA, van der Gucht J. Binodal compositions of polyelectrolyte complexes. *Macromolecules*. 2010;43(15):6476–6484.
39. Deac A, Qi Q, Indulkar AS, et al. Dissolution mechanisms of amorphous solid dispersions: role of drug load and molecular interactions. *Mol Pharm*. 2023;20(1):722–737.
40. Indulkar AS, Gao Y, Raina SA, Zhang GG, Taylor LS. Exploiting the phenomenon of liquid-liquid phase separation for enhanced and sustained membrane transport of a poorly water-soluble drug. *Mol Pharmaceutics*. 2016;13(6):2059–2069.
41. Narasimhan B, Peppas NA. On the importance of chain reptation in models of dissolution of glassy polymers. *Macromolecules*. 1996;29(9):3283–3291.
42. Wilson VR, Mugheirbi NA, Mosquera-Giraldo LI, et al. Interaction of polymers with enzalutamide nanodroplets—impact on droplet properties and induction times. *Mol Pharm*. 2021;18(3):836–849.
43. Ueda K, Higashi K, Moribe K, Taylor LS. Variable-temperature NMR analysis of the thermodynamics of polymer partitioning between aqueous and drug-rich phases and its significance for amorphous formulations. *Mol Pharm*. 2021;19(1):100–114.
44. Ueda K, Moseson DE, Pathak V, Taylor LS. Effect of polymer species on maximum aqueous phase supersaturation revealed by quantitative nuclear magnetic resonance spectroscopy. *Mol Pharm*. 2021;18(3):1344–1355.
45. Ortega-Vinuesa J, Martın-Rodrıguez A, Hidalgo-Alvarez R. Colloidal stability of polymer colloids with different interfacial properties: mechanisms. *J Colloid Interface Sci*. 1996;184(1):259–267.
46. Napper DH. Steric stabilization. *J Colloid Interface Sci*. 1977;58(2):390–407.
47. Li Z, Shakiba S, Deng N, Chen J, Louie SM, Hu Y. Natural organic matter (NOM) imparts molecular-weight-dependent steric stabilization or electrostatic destabilization to ferrihydrite nanoparticles. *Environ Sci Technol*. 2020;54 (11):6761–6770.
48. Colby RH, Fetters LJ, Graessley WW. The melt viscosity-molecular weight relationship for linear polymers. *Macromolecules*. 1987;20(9):2226–2237.